



Comparative study of nucleation and growth mechanism of cobalt electrodeposited on ITO substrate in nitrate and chloride electrolytes

J. Bahar¹ · Y. Lghazi¹ · B. Youbi¹ · M. Ait Himi¹ · I. Bimaghra¹

Received: 22 December 2020 / Revised: 22 April 2021 / Accepted: 25 April 2021 / Published online: 5 May 2021
© The Author(s), under exclusive licence to Springer-Verlag GmbH Germany, part of Springer Nature 2021

Abstract

A comparative study of the electrochemical deposition of cobalt on tin-doped indium oxide (ITO) substrate was carried out using electrochemical techniques in nitrate and chloride electrolytes. The bath used for the study in a nitrate medium contains 0.01 M of cobalt nitrate hexahydrate ($\text{Co}(\text{NO}_3)_2 \cdot 6\text{H}_2\text{O}$) with 0.1 M of potassium nitrate (KNO_3). For the chloride medium study, the electrolyte consists of a mixture of 0.01 M CoCl_2 with 0.1 M potassium chloride (KCl). The cyclic voltammetry (CV) and the chronoamperometry (CA) have been used to study the kinetics, nucleation, and growth mechanism. The (CV) and (CA) measurements revealed that the electrodeposition of cobalt (Co) at a negative potential around -0.95 V versus SCE (saturated calomel electrode) is a quasi-reversible reaction controlled by the diffusion process in the two electrolytes. The measured current transient curves were compared to those calculated from Scharifker-Hills and Heerman-Tarallo models. It was found that a progressive three-dimensional (3D) nucleation mechanism governed the nucleation and the growth of Co on the ITO substrate in chloride solution, while in nitrate solution, the nucleation mechanism followed the instantaneous 3D model. The characterization of samples by X-ray diffraction had shown that the cobalt electrodeposited on ITO substrate has a hexagonal crystal structure whatever the electrolyte composition.

Keywords Cobalt · Electrodeposition · Cyclic voltammetry · Chronoamperometry · Nucleation and growth

Introduction

Cobalt is a transition metal that belongs to the iron triad group in the periodic table. It is a relatively rare magnetic element with properties similar to iron and nickel. Recently, because of its magnetic and structural properties [1], nanostructured materials based on cobalt have many applications, such as the production of chemical sensors [2], cathodes for alkaline-hybrid batteries [3], catalysts for hydrolysis and hydrogen evolving reactions [4], electro-catalyzed reactions [5], lithium-ion batteries, superconducting magnets, and the aerospace industry [6]. The many synthetic routes have been developed to produce cobalt nanostructures with different morphologies as nanowires [7], nanotubes, nanodisks, nanosheets, and nanoplatelets [8]. These large applications are

due to the cobalt properties which have also been improved by substitution and combination with other elements such as Bi, Al, Ge, and In [9]. The substitution of cobalt (Co) in intermetallic compounds induces important modifications on their structural and magnetic properties, knowing that the increase in the rate of substitution of cobalt (Co) is accompanied with the variation of the mesh parameters [9]. Several physical and chemical methods have been used to develop cobalt film, in particular, sol-gel, spray pyrolysis, laser ablation, and electrodeposition. This latter appears simple and less expensive compared to the other techniques that require sophisticated materials. Also, it allows controlling the physicochemical properties of materials by a simple change of the deposition parameters such as pH, the composition of the electrolyte, bath temperature, and electrodeposition potential [10]. Besides, the study of the kinetic, nucleation, and growth mechanism of the metal crystals formed on the substrate allows to determine the different physicochemical properties [11]. In this work, we are particularly interested to study the effect of the electrolyte composition (chloride and nitrate) on the nucleation and growth mechanism of cobalt deposited on ITO substrate at room temperature.

✉ J. Bahar
Jihanebahar63@gmail.com

¹ Bio-Geosciences and Materials Engineering Laboratory, Ecole Normale Supérieure, Hassan II University of Casablanca, Casablanca, Morocco

Experimental

Electrodeposition

The electrochemical measurement was performed using three electrodes cell configuration connected to VersaStat3 potentiostat/galvanostat assisted by a computer using the versa studio software. ITO (tin (Sn)-doped indium oxide (In_2O_3)) substrate with a surface area of 1 cm^2 was used as a working electrode. Glassy carbon electrode of disc-shaped (1.5 cm in diameter) was used as a counter electrode and saturated calomel electrode (SCE) as a reference electrode (all potentials were given versus SCE). The counter electrode had been placed parallel to the ITO substrate at a distance of 1 cm. Before the electrodeposition experiences, the ITO substrate surface was ultrasonically cleaned using an acetone bath and then with distilled water.

The cobalt films were electrodeposited from the both electrolyte medium: the first one (nitrate medium) contained cobalt nitrate hexahydrate $\text{Co}(\text{NO}_3)_2 \cdot 6\text{H}_2\text{O}$ (0.01 M) with potassium nitrate KNO_3 (0.1 M) and the second one (chloride medium) contained cobalt chloride CoCl_2 (0.01 M) with potassium chloride KCl (0.1 M). All chemicals were of reagent grade and were used without further purification. All solutions were prepared with distilled water. The pH value in the two electrolytes is approximately 6. All the experiments were carried out at 25 °C.

Characterization

The structure of the thin films of cobalt (Co) were determined by X-ray diffraction (XRD) analysis, using a Broker D8 Advance diffractometer, equipped with a graphite monochromator, a Lynx-Eye detector, and parallel beam optics $\text{Cu K}\alpha$ radiation ($\lambda = 1.5411\text{ \AA}$).

Results and discussion

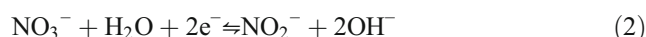
Cyclic voltammetry

The cyclic voltammetry study, potentiodynamic measurement, of the different electrolytic solutions allowed in the one hand to determine the redox potentials of cobalt deposition and on the other hand to characterize the reversibility of the system and the electrodeposition mechanism. In this technique, the working electrode potential ramped linearly versus time with a well-determined scanning rate.

To study the electrochemical behavior of the ITO substrate in the supporting electrolytes and to identify the different redox reactions related to the cobalt ions involved in the two mediums, the cyclic voltammetry measurements were carried out in potassium nitrate (0.1 M) and potassium chloride (0.1

M) solutions with and without the cobalt ions (CoCl_2 or $\text{Co}(\text{NO}_3)_2 \cdot 6\text{H}_2\text{O}$ (0.01 M)). The potential range used for nitrate medium was 1.5 to -1.4 V/SCE and for the chloride solution was 0 to -1.2 V/SCE . The obtained voltammograms with a scan rate of 50 mV s^{-1} were represented in Fig. 1.

We noted first of all, in nitrate and chloride blanks (inset Fig. 1), the substrate stability in all the range potential used. The anodic system observed in nitrate solution can be attributed to the water oxidation. However, the cathodic reduction system observed in the both solution corresponds to water reduction (Eq. 1) according to Eq. (1), and in nitrate medium, this reduction is accompanied by the nitrate reduction (Eq. 2).

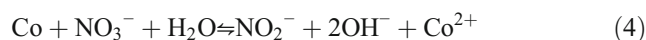


A crossover of the reverse anodic scan over the cathodic scan (nucleation loop) was observed for the two mediums, which was indicated by the formation of Co nuclei on the ITO substrate [12]. Then, in nitrate medium (Fig. 1a) during the sweep of the cathodic potentials, we had observed a reduction peak corresponding to the reduction of Co(II) to Co(0) according to the reaction (3) that occurred in the proximity of potential -0.95 V/SCE as indicated in the literature [13].



During the return scan, an anodic peak was observed at $E \approx 0.8\text{ V/SCE}$ which corresponded to the dissolution (oxidation) of the cobalt deposited during the cathodic part.

Moreover, in the nitrate medium the formation of cobalt oxide (CoO) is also possible. The electrochemical formation mechanism of CoO is known to be initiated by the reduction of nitrate ions that produces hydroxide ions, followed by the precipitation of $\text{Co}(\text{OH})_2$. Then, $\text{Co}(\text{OH})_2$ is converted to CoO. The sequence of the CoO deposition can be summarized by the following Eqs. (4), (5), and (6):



In the chloride bath (Fig. 1b), the reduction of cobalt (II) according to reaction (3) was observed at $E \approx -0.95\text{ V/SCE}$ and the cobalt dissolution was around -0.15 V/SCE .

The reversibility of the cobalt redox system was studied using the effect of the scan rate. Figure 2a and b had shown the voltammograms obtained at different scan rates for the both electrolytes (chloride and nitrate).

We found that as the scan rate increased, the cathodic peaks became more intense and have shifted to the negative values. Similarly, in the anodic zone, the intensity of oxidation peaks increases with the scan rate and the corresponding potentials

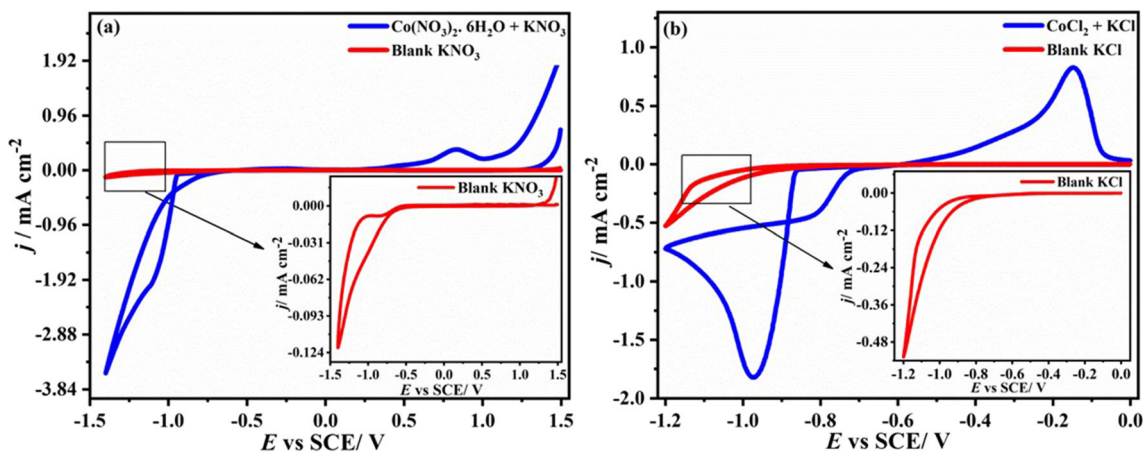


Fig. 1 Cyclic voltammograms for Co electrodeposition on ITO substrate and supporting electrolytes (Blanks) at scan rate 50 mV s^{-1} : **a** from nitrate solution and **b** from chloride solution

were shifted to the more positive values. As can be seen from Tables 1 and 2, for all the cyclic voltammograms, the difference between the potential peak E_p and the half potential peak $E_{p/2}$ is larger than the theoretical value of $2.2RT/nF$ for reversible reaction [14].

We also note that the $|(E_{pc}+E_{pa})/2|$ value varies slightly with the scan rate; this indicates that the Co^{2+}/Co is a quasi-reversible system [14].

Chronoamperometry

In order to study the nucleation and growth mechanism of cobalt electrodeposition on ITO substrate from chloride and nitrate electrolytes, chronoamperometry is employed. Then the potential of the working electrode is stepped and the resulting current is monitored as a function of time [15, 16].

Current density-time transients

Figure 3a and b had shown a series of current density-time transients obtained at different potentials of cobalt deposition

from the nitrate (a) and chloride (b) mediums. These deposition potentials correspond to the cathodic peak domain according to the voltammograms of Fig. 1

It can be seen that for each potential, the current density-time transients have almost the same behavior. We can say that they all have a typical transient appearance in the case of a three-dimensional growth controlled by the diffusion [17]. Indeed, three parts have been identified in each curve. The first part is when the current decay corresponds to the double layer charge and the formation of the first germs on the active sites of the substrate surface. Then, in the ascending part, the current density increases rapidly reaching a maximum j_{max} at a given time t_{max} due to the formation and growth of cobalt nuclei. In this latter region, the current density maximum (j_{max}) increases while the corresponding t_{max} time decreases with increasing the applied potential as a consequence of the higher nucleation density. From chloride solution shown in Fig. 3b, the transients showed a descending part attributed to the intervention of a diffusion process. Therefore, after the maximum $t > t_{max}$ current of this transient remained constant. Contrary, the transient curves obtained from nitrate solution

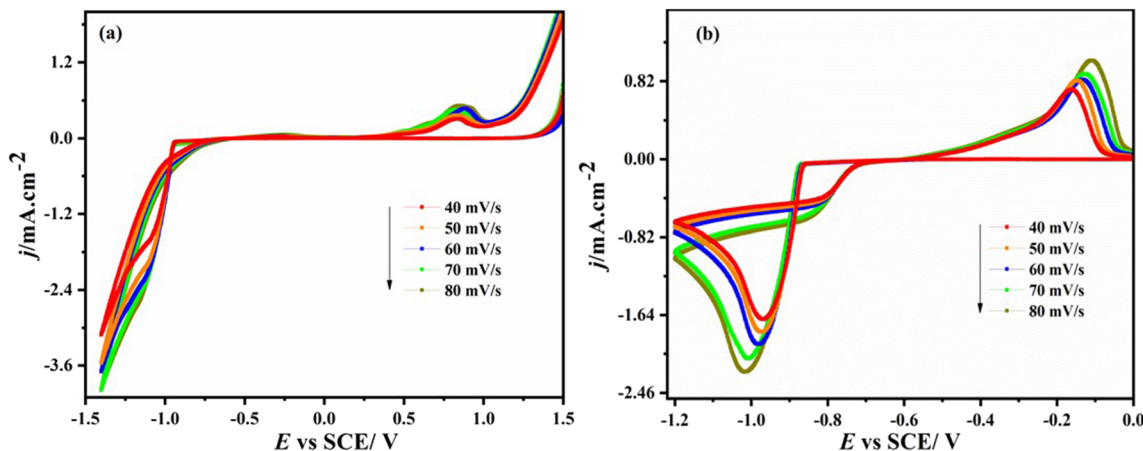


Fig. 2 Cyclic voltammograms for Co electrodeposition on ITO substrate at different scan rates: **a** from nitrate solution and **b** from chloride solution

Table 1 Current density, cathodic and anodic peak potential as a function of scanning speed deduced from voltammograms the nitrate medium

v (mV s ⁻¹)	E_{pc} (V)	J_{pc} (mA cm ⁻²)	$J_{pc}/2$ (mA cm ⁻²)	$E_{pc}/2$ (V)	E_{pa} (V)	$ E_{pc} - E_{pc}/2 $ (V)	$ (E_{pc} + E_{pa})/2 $ (V)
40	-1.0828	-1.5937	-0.7968	-0.9897	0.8317	0.0931	0.1255
50	-1.0944	-2.0045	-1.0023	-0.9952	0.8379	0.0992	0.1282
60	-1.1115	-2.1512	-1.0756	-1.0014	0.8782	0.1101	0.1166
70	-1.1231	-2.3411	-1.1705	-1.0068	0.8030	0.1163	0.1600
80	-1.1580	-2.6345	-1.3172	-1.0246	0.8728	0.1334	0.1426

(Fig. 3a) showed that the diffusion limit current increases with the applied potential; this behavior may be caused by the existence of an additional process to the nucleation and growth process of cobalt. It is possible to consider that such additional process is due to the proton reduction process accompanied with the nitrate ions reduction according to Eq. (2) [18]. Moreover, another electrochemical reaction can be taken into consideration. In the nitrate medium, the cobalt metal thus formed can react chemically with nitrate ions to give a cobalt oxide (CoO) [19] according to Eqs (4), (5), and (6).

Analysis of the descending part of the transients

In order to verify the nucleation mechanism process control by the exploitation of the last part of the transients, we have traced the evolution of current density (j) versus $t^{-1/2}$.

The series of curves given the transients current density (j) as a function of $t^{-1/2}$ was drawn as shown in Fig. 4a and b. These curves represented a good linear relationship between (j) and $t^{-1/2}$ which is a typical three-dimensional (3D) nucleation with diffusion-controlled growth according to Cottrell Eq. (7) [20, 21].

The diffusion coefficient D can be deduced from the slopes of the curves on Fig. 4a and b according to the Cottrell equation:

$$j(t) = nFC \left[\frac{D}{\pi t} \right]^{1/2} \quad (7)$$

where nF is the molar charge transferred during electrodeposition ($F = 96500 \text{ C}\cdot\text{mol}^{-1}$), C is the bulk concentration of the electroactive species (mol L^{-1}), D is the diffusion coefficient ($\text{cm}^2 \text{ s}^{-1}$), and t is time (s).

Table 2 Current density, cathodic and anodic peak potential as a function of scanning speed deduced from voltammograms the chloride medium

v (mV s ⁻¹)	E_{pc} (V)	J_{pc} (mA cm ⁻²)	$J_{pc}/2$ (mA cm ⁻²)	$E_{pc}/2$ (V)	E_{pa} (V)	$ E_{pc} - E_{pc}/2 $ (V)	$ (E_{pc} + E_{pa})/2 $ (V)
40	-0.9674	-1.6648	-0.8324	-0.8939	-0.1627	0.0367	0.5650
50	-0.9747	-1.8421	-0.9210	-0.8987	-0.1438	0.0380	0.5592
60	-0.9794	-1.9406	-0.9703	-0.9012	-0.1274	0.0391	0.5534
70	-1.0078	-2.0889	-1.0444	-0.9129	-0.1249	0.0474	0.5663
80	-1.0172	-2.2361	-1.1180	-0.9154	-0.1085	0.0509	0.5628

Tables 3 and 4 show the diffusion coefficient calculated using the Cottrell equation and the transients obtained from nitrate and chloride solution, respectively, for different applied potential. The D average value in nitrate medium is about $0.33 \cdot 10^{-6} \text{ cm}^2 \text{ s}^{-1}$ and $1.67 \cdot 10^{-6} \text{ cm}^2 \text{ s}^{-1}$ in chloride medium.

Therefore, we can be concluded that the diffusion coefficient D is slightly dependent of the applied potential and it is higher in a medium containing Cl^- ions compared to that of NO_3^- .

Analysis of the ascending part of the transients

The Astley approach can be considered to characterize the nucleation mode of the first stage of electro crystallization by plotting $j(t) = f(t^{1/2})$ and $j(t) = f(t^{3/2})$ of ascending part of current transients ($t < t_{\text{max}}$) [22, 23]. These theoretical models had described the 3D nucleation mechanism using the variation of the current density in the second part on the current transients according to the following equations:

$$\begin{aligned} \text{For instantaneous 3D nucleation : } j(t) \\ = nF\pi(2DC)^{3/2}(M/\rho)^{1/2}Nt^{1/2} \end{aligned} \quad (8)$$

$$\begin{aligned} \text{For progressive 3D nucleation : } j(t) \\ = \frac{2}{3} nF\pi(2DC)^{3/2}(M/\rho)^{1/2}ANt^{3/2} \end{aligned} \quad (9)$$

where $j(t)$ is the current density (A cm^{-2}), C is the concentration of the electroactive ions (mol cm^{-3}), D is the diffusion coefficient ($\text{cm}^2 \text{ s}^{-1}$), F is the faraday constant ($96,500 \text{ C mol}^{-1}$), n is the number of electron transferred in the electro-deposition process, M is the molar mass of the deposit (g

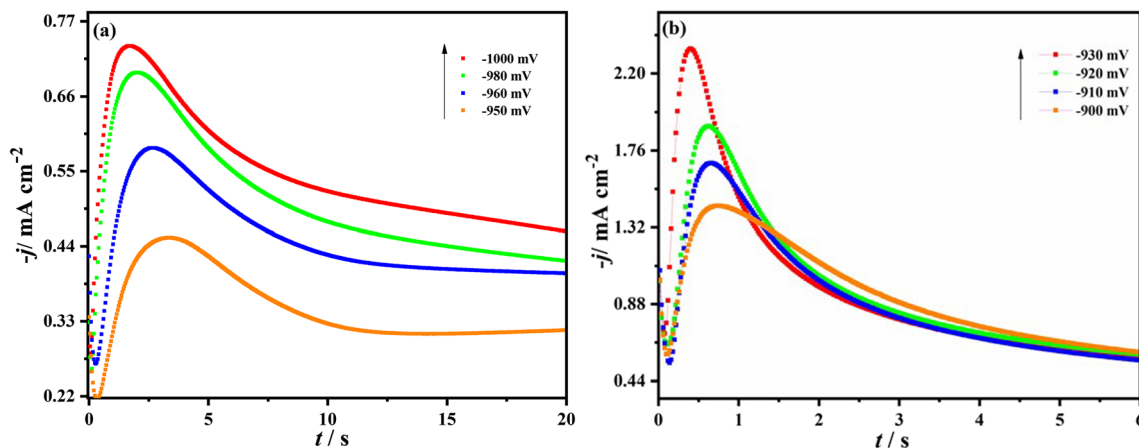


Fig. 3 Transients current density for Co electrodeposition on ITO substrate at different deposition potentials: **a** in nitrate solution and **b** in chloride solution

mol^{-1}), ρ is the density of the deposit (g cm^{-3}). A is the nucleation rate constant (s^{-1}), and N is the number density of nuclei (cm^{-2}).

The instantaneous nucleation means that all active sites nucleation on the surface are filled at the same time; the curve of $j(t) = f(t^{1/2})$ must be linear. Thus, at progressive nucleation, the new germs are continuously created during the electrodeposition time and the $j(t) = f(t^{3/2})$ is a linear curve [21, 23].

According to Eqs. (8) and (9), for all the transients that are presented in Fig. 3a and b, the experimental currents density of the second part were plotted versus $t^{1/2}$ and $t^{3/2}$ in Figs. 5 and 6. As can be observed from Fig. 5, the plots (j) versus $t^{1/2}$ (Fig. 5a) display a good linear relationship for all applied potential with a high correlation factors compared to the plots (j) versus $t^{3/2}$ (Fig. 5b). This implies that the electrochemical deposition of cobalt (Co) from nitrate electrolyte exhibits probably instantaneous 3D nucleation [21]. However, Fig. 6 shows that the current increases linearly with $t^{1/2}$ (Fig. 6a) also with $t^{3/2}$ (Fig. 6b) with correlation factors $R^2 \geq 0.984$. As a result, the nucleation mechanism of cobalt on ITO substrate

from chloride solution cannot be revealed directly from these plots. Hence, there is the need to use another model.

Non-dimensional curves $(j/j_{\text{max}})^2$ versus t/t_{max}

Scharifker and Hills have proposed a theoretical model that allows verifying the type of nucleation of deposit. These equations are related to current density and the time, and are given by the following equations [23, 24]:

$$\begin{aligned} \text{For instantaneous 3D nucleation : } & \left(\frac{j}{j_{\text{max}}}\right)^2 \\ & = 1.9542 \frac{t_{\text{max}}}{t} \left[1 - \exp\left(-1.2564 \frac{t}{t_{\text{max}}}\right) \right]^2 \end{aligned} \tag{10}$$

$$\begin{aligned} \text{For progressive 3D nucleation : } & \left(\frac{j}{j_{\text{max}}}\right)^2 \\ & = 1.2254 \frac{t_{\text{max}}}{t} \left[1 - \exp\left(-2.3367 \left(\frac{t}{t_{\text{max}}}\right)^2\right) \right]^2 \end{aligned} \tag{11}$$

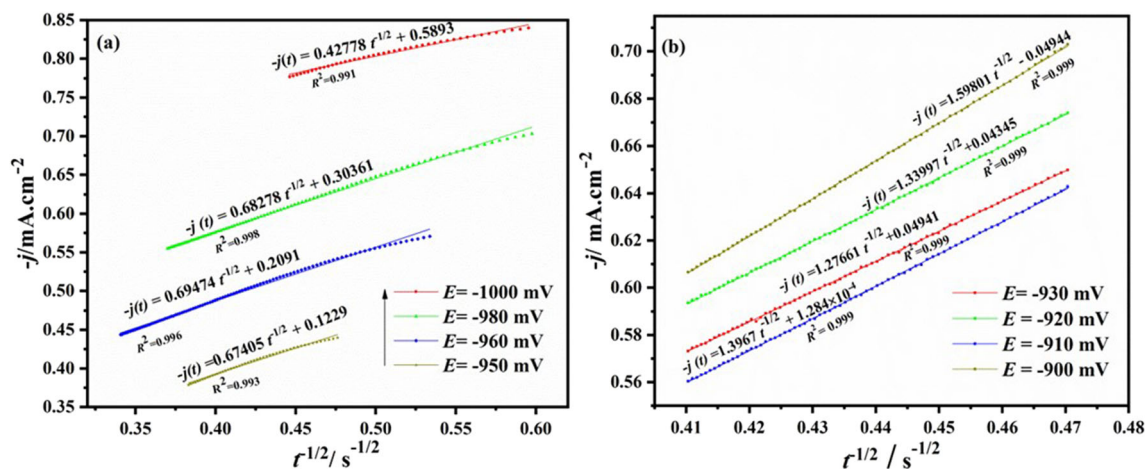


Fig. 4 Transients current density (j) versus $t^{-1/2}$ of the last part at different potentials: **a** from nitrate solution and **b** from chloride solution

Table 3 Diffusion parameter D of Cobalt electrodepositing on ITO substrate from electrolyte $\text{Co}(\text{NO}_3)_2 \cdot 6\text{H}_2\text{O}$ 0.01 M, and KNO_3 0.1 M at different potentials

E (mV/SCE)	D ($\times 10^{-6}$ $\text{cm}^2 \text{s}^{-1}$)
-1000	0.15
-980	0.39
-960	0.41
-950	0.38

Table 4 Diffusion parameter D of cobalt electrodepositing on ITO substrate from electrolyte CoCl_2 0.01 M and KCl 0.1 M at different potentials

E (mV/SCE)	D ($\times 10^{-6}$ $\text{cm}^2 \text{s}^{-1}$)
-930	1.37
-920	1.51
-910	1.64
-900	2.15

Figure 7 shows a comparison between the transients of the experimental curves at different potentials during the electrodeposition of cobalt, with the theoretical dimensionless transients of $(j/j_{\text{max}})^2$ versus t/t_{max} .

We noted that the transients of cobalt in nitrate electrolyte (Fig. 7a) are following the three-dimensional (3D) instantaneous nucleation mode [20, 25] with a good agreement in the first part ($t/t_{\text{max}} \leq 1$). However, a deviation of the experimental data in comparison to the theoretical curves is observed in the second part ($t/t_{\text{max}} \geq 1$). This behavior may be caused by the existence of an additional process to the nucleation and growth process of cobalt. It is possible to consider that such an additional process is due to the proton reduction process [18]. Moreover, another electrochemical reaction can be taken into consideration. In the nitrate medium, the cobalt metal thus formed can react chemically with nitrate ions to give a cobalt

oxide (CoO) [19]. Figure 7b shows that all of the experimental curves obtained in chloride electrolyte are in good agreement with progressive nucleation. In this case, the little difference between the theoretical and the experiments plots is probably due to the nuclei forms knowing that the theoretical models are developed for the nuclei with hemispherical geometry [26].

As a conclusion, these analyses showed that the nucleation mechanism of cobalt deposition on ITO substrate changes from one medium to the other without being influenced by the deposition potential.

Kinetic parameters of the cobalt electrodeposition

Scharifker and Hills model

According to Scharifker and Hills model for instantaneous and progressive nucleation, we have determined from the maximum current density and the corresponding times in transients the following kinetic parameters: the number of active nucleation sites N_0 , the diffusion coefficient D , and the nucleation rate constant A according to the equations described in Table 5 [27].

For the instantaneous nucleation, the kinetics parameters A , D , and N_0 are calculated using Eqs. (12), (13), and (14), respectively. The obtained values are regrouped in the Table 6.

For progressive nucleation, from the chloride solution, the kinetics parameters of nucleation D and the product of $A \cdot N_0$ are calculated according to Eqs. (15) and (16) and represented in Table 7.

For the all cases, we noted that the increase of applied potential was associated with the increase of maximal current, the nucleation rate A , nuclei density N_0 , and the product $A \cdot N_0$. This behavior is typical for 3D nucleation and growth of a new phase under diffusion control. However, the diffusion

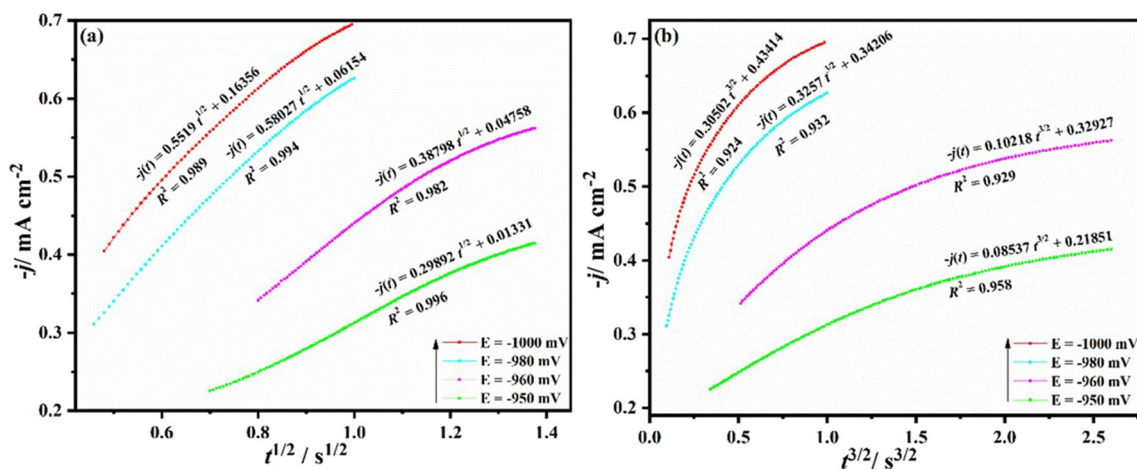


Fig. 5 a Transients current density (j) versus $t^{1/2}$ of the second part at different potentials and b transients current density (j) versus $t^{3/2}$ of the first part at different potentials in nitrate solution

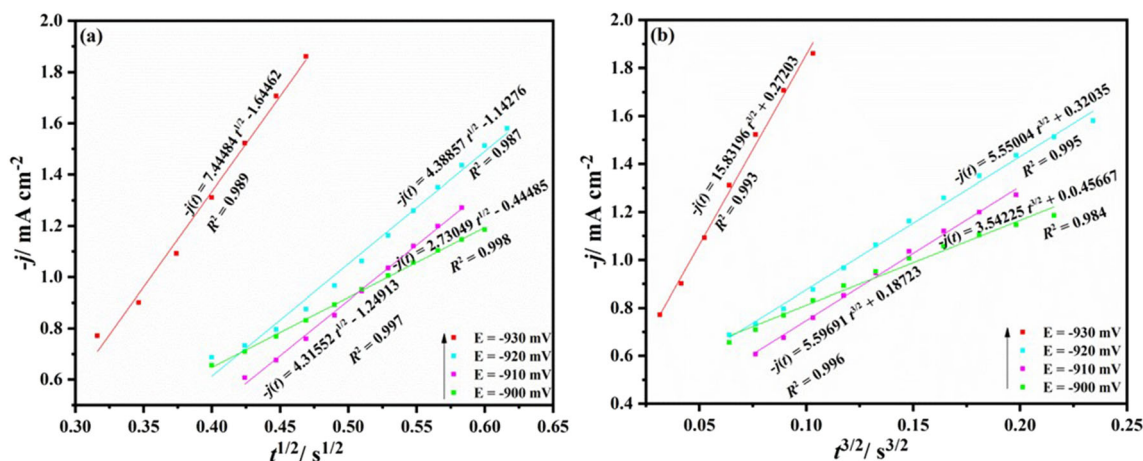


Fig. 6 **a** Transients current density (j) versus $t^{1/2}$ of the second part at different potentials and **b** transients current density (j) versus $t^{3/2}$ of the first part at different potentials in chloride solution

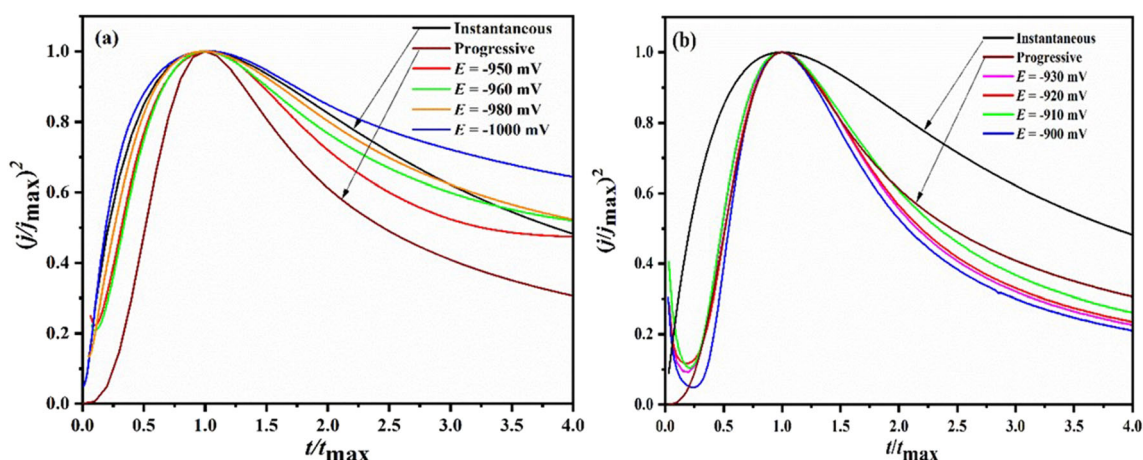


Fig. 7 Comparison of theoretical non-dimensional $(j/j_{max})^2$ versus (t/t_{max}) plots for instantaneous nucleation from Eq. (10) and progressive nucleation from Eq. (11) to experimental transients current density of different potentials: **a** in nitrate solution and **b** in chloride solution

coefficient evolution is related to the electrolyte composition; it increases with the applied potential in the chloride solution and decreases in the nitrate solution. Considering that with this model, the A and N_{∞} cannot be calculated separately, the comparison of the Kinetic parameters is not possible.

Heerman-Tarallo model

In order to extract quantitative information on the kinetics mechanism associated with the Cobalt nucleation and growth process, the model of Heerman-Tarallo [28] was

Table 5 Expression of the kinetic parameters for instantaneous and progressive nucleation

Instantaneous nucleation	Progressive nucleation
$D = \frac{j_{max} t_{max}}{0.1629(nFC)^2}$ (12)	$D = \frac{j_{max}^2 t_{max}}{0.2598(nFC)^2}$ (15)
$N0 = 0.065 \left(\frac{8\pi CM}{\rho} \right)^{-1/2} \left(\frac{nFC}{j_{max} t_{max}} \right)^2$ (13)	$AN_{\infty} = \frac{0.3866 j_{max} (nFC)^2}{\frac{4}{3} \left(\frac{8\pi CM}{\rho} \right)^{1/2} t_{max}^3}$ (16)
$A = N0\pi \left(\frac{8\pi CM}{\rho} \right)^{1/2} D$ (14)	

Table 6 Values of j_{\max} , t_{\max} , N_0 , D , and A at different potentials, calculated from Eqs. (12), (13), and (14), at nitrate solution

E (mV/SCE)	$-j_{\max}$ (mA/cm ²)	t_{\max} (s)	D ($\times 10^{-6}$ cm ² s ⁻¹)	N_0 ($\times 10^6$ cm ⁻²)	A (s ⁻¹)
-1000	0.8574	1.92	1.11	2.19	0.65
-980	0.6946	2.04	1.51	2.32	0.61
-960	0.5843	2.04	1.62	2.42	0.47
-950	0.4526	3.29	2.33	2.68	0.38

Table 7 The values of j_{\max} , t_{\max} , D and AN_s at different potentials, calculated from Eqs. (15) and (16), at chloride solution

E (mV/SCE)	$-j_{\max}$ (mA/cm ²)	t_{\max} (s)	D ($\times 10^{-6}$ cm ² s ⁻¹)	AN_s (cm ⁻² s ⁻¹)
-930	2.3436	0.39	2.21	1.046
-920	1.9021	0.62	2.32	0.211
-910	1.6789	0.65	1.89	0.162
-900	1.4500	0.73	1.58	0.098

used as a convenient method to identify the typical kinetics parameters. According to this model, which merges the approaches of Scharifker-Mostany [29] and Sluyter-Rehbach [30], the nucleation rate constant (A) and the number density of active sites (N_0) can be fitting the entire experimental current transient to the following expression [28]:

$$j(t) = nFDC(\pi Dt)^{-1/2} \frac{\phi}{\theta} \left\{ 1 - \exp\left[-\alpha N_0(\pi Dt)^{1/2} t^{1/2} \theta\right] \right\} \quad (17)$$

$$\phi = 1 - \frac{\exp(-At)}{(At)^{1/2}} \int_0^{(At)^{1/2}} \exp(\lambda^2) d\lambda \quad (18)$$

$$\theta = 1 - \frac{\exp(-At)}{(At)} \quad (19)$$

$$\alpha = 2\pi \left(\frac{2MDC}{\rho} \right)^{1/2} \quad (20)$$

where n is the number of electrons involved in the chemical reaction, F is the Faraday's constant, nF is the molar charge transferred during electrodeposition, D is the diffusion coefficient, C is the metal ion concentration, M is the molar mass, and ρ is the density of the Cobalt deposit. The function ϕ is directly related to the

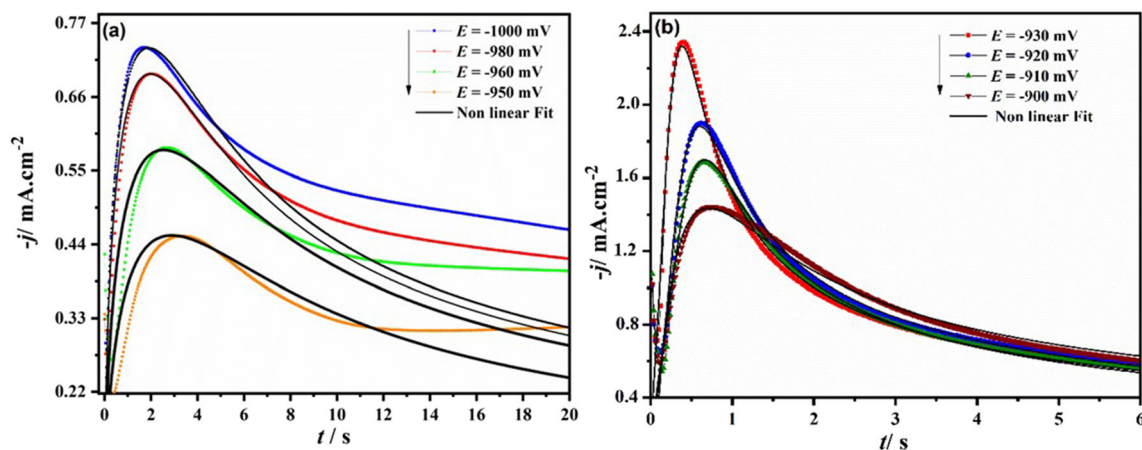


Fig. 8 Comparison between the experimental current transients and the corresponding theoretical current transients (black line) obtained by nonlinear fitting Eq. (10) to the experimental data from **a** nitrate solution and **b** chloride solution

Table 8 Kinetic parameters of the cobalt electrodepositing on ITO substrate from electrolyte $\text{Co}(\text{NO}_3)_2 \cdot 6\text{H}_2\text{O}$ 0.01 M, and KNO_3 0.1 M at different potential

E (mV/SCE)	A (s^{-1})	N_0 ($\times 10^7 \text{cm}^{-2}$)	D ($\times 10^{-6} \text{cm}^2 \text{s}^{-1}$)
-1000	8	3.46	1.68
-980	7	3.26	1.56
-960	5	3.20	1.40
-950	2	3.07	0.98

Table 9 Kinetic parameters of the cobalt electrodepositing on ITO substrate from electrolyte CoCl_2 0.01 M and KCl 0.1 M at different potential

E (mV/SCE)	A (s^{-1})	N_0 ($\times 10^7 \text{cm}^{-2}$)	D ($\times 10^{-6} \text{cm}^2 \text{s}^{-1}$)
-930	3.17	5.56	5.81
-920	2.25	3.06	5.69
-910	2.04	2.61	6.13
-900	1.6	2.21	6.47

Dawson’s integral and reflects the retardation of the current by slow nucleation, and θ reflects the retardation of the growth of the coverage as a result of slow nucleation [31]. Equation (18) has some mathematical complexity due to the presence of Dawson’s integral in calculating the kinetics parameters. Using the function $F(x) = \exp(-x^2) \int_0^x \exp(\lambda^2) d\lambda$ can be efficiently approximated with the polynomial [32]:

$$F(x) = \frac{0.051314213 + 0.47910725x}{1 - 1.2068142x + 1.185724x^2} \tag{21}$$

Equation (17) can be rewritten as:

$$\phi = \frac{0.52089275 - 1.2068142(At)^{1/2} + 1.185724(At) - 0.051314213(At)^{-1/2}}{1 - 1.2068142(At)^{1/2} + 1.185724(At)} \tag{22}$$

As it is shown in Fig. 8a, from nitrate solution, the Heerman-Tarallo theoretical curves are correlated to the experimental curves specialty in the first part. The deviation observed in the last part of the current transients confirms that the cobalt electrode position from the nitrate medium was accompanied by an additional process (nitrate and hydrogen reduction). However, from chloride solution (Fig. 8b), the nonlinear fitting curves are in good agreement with the experimental transient curves.

Then, this model can be applied with sufficient accuracy to extract the kinetics parameters, A , N_0 , and D . The obtained values are listed in Tables 8 and 9 for nitrate and chloride solution.

We have concluded that A and N_0 increase whatever the electrolyte composition, while the diffusion coefficient increases for nitrate solution and decreases for the chloride solution with applied potential. The diffusion coefficient can be considered unchanged with applied potential; the D average is about $6.025 \times 10^{-6} \text{cm}^2 \text{s}^{-1}$ in nitrate solution and $1.405 \times 10^{-6} \text{cm}^2 \text{s}^{-1}$ in chloride solution. Similar results have been also found in several papers [33, 34]. The behavior of A and N_0 indicates the existence of energy distribution on the surface with a larger fraction of sites that is becoming active with the increase of the deposition potential [33].

Crystal structure determination

The deposited film from nitrate solution has cyan color; however, using the chloride solution, the electrodeposited cobalt has a blue color.

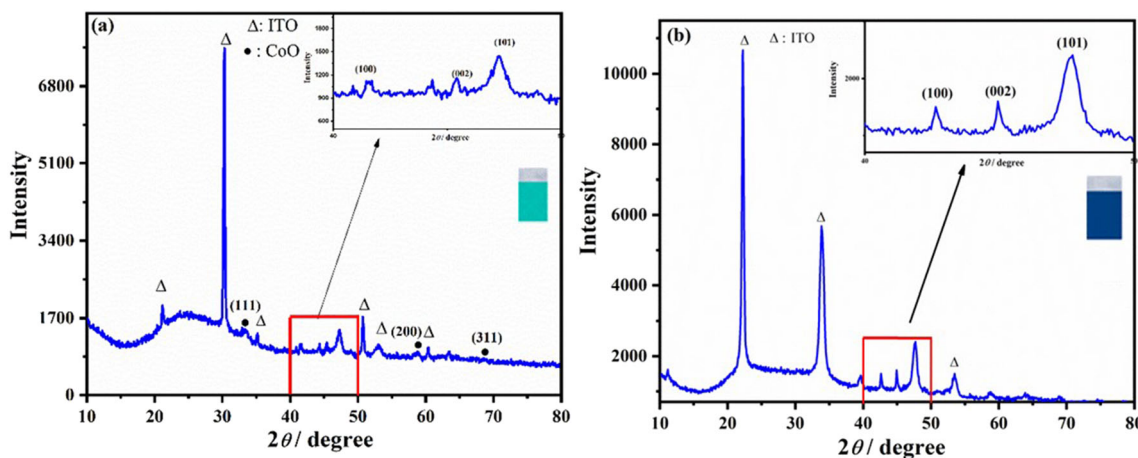


Fig. 9 X-ray diffraction patterns of Cobalt thin film. **a** In nitrate solution and **b** in chloride solution

Table 10 Calculate the grain size of cobalt layers on ITO substrate in nitrate solution at potential -0.97 V

2θ (°)	FWHM (°)	<i>hkl</i>	<i>d</i> -spacing (Å)	<i>D</i> (Å)
41.887	0.94466	100	2.1552	90.0750
45.792	0.83165	002	1.9805	103.7279
47.354	1.11137	101	1.9202	78.0774

The X-ray diffraction patterns of the elaborated sample with electrodeposition method, on ITO substrate realized at -0.97 V/SCE from nitrate solution and -0.92 V/SCE from chloride solution, are shown in Fig. 9.

As can be seen, the diffractograms of cobalt electrodeposited from nitrate and chloride solution present the same peaks. The diffraction peaks at $2\theta = 41.887^\circ$, 45.792° , and 47.354° are characteristic of hexagonal cobalt (Co) which orientations have been preferred (100), (002), and (101) at two electrolytes. Moreover, in the nitrate medium, new diffraction peaks are observed at $2\theta = 34.149^\circ$, 58.30° , and 68.425° which can be attributed to a new phase that has been formed. According to the literature, these diffraction peaks are characteristic of cobalt oxide (CoO) whose orientations were preferred (111), (200), and (311) [35, 36]. These results are in good agreement with those reported in other studies of cobalt electrodeposition film [35, 36]. The appearance of some XRD peaks reflections corresponding to ITO substrate.

The physical properties of materials are intrinsically related to the grain size. Therefore, the study of grain size has a considerable importance. Thus, the magnetic properties depend on the grain size [37]. The Scherer equation was used to estimate the particles size from the XRD pattern of the as prepared nanoparticles [38]:

$$D = \frac{k\lambda}{\beta \cos\theta} \quad (23)$$

where λ is the wavelength of the incident radiation ($\lambda = 1.5411 \text{ \AA}$), $k = 0.9$, β is the full width at half maximum (FWHM) of the preferentially oriented diffraction peak, and θ is the Bragg diffraction angle.

Table 11 Calculate the grain size of cobalt layers on ITO substrate in chloride solution at potential -0.92 V

2θ (°)	FWHM (°)	<i>hkl</i>	<i>d</i> -spacing (Å)	<i>D</i> (Å)
41.6788	0.3483	100	2.16708	244.1324
44.4805	0.2903	002	2.03687	295.7490
47.4319	0.6967	101	1.91679	124.5856

Tables 10 and 11 show the variation of crystallite size values of cobalt electrodeposited from nitrate and chloride solution, respectively.

Tables 10 and 11 indicate that the crystallite size of cobalt electrodeposited on ITO substrate strongly depended on the solution composition; the average size value is 90.63 \AA and 221.49 \AA from nitrate and chloride solution, respectively.

Conclusion

To sum up, the present work was dedicated to studying the effect of electrolyte composition (nitrate and chloride) on the electrodeposition mechanism of cobalt on ITO substrate. First, the cyclic voltammetry has shown that the electrodeposition process from the two mediums is a quasi-reversible reaction; this latter has accompanied by the hydrogen and the nitrate reduction in the case of electrodeposition from the nitrate medium. The chronoamperometry method showed that the electrodeposition nucleation mechanism strongly depended on the electrolyte composition. The Scharifker-Hills model has confirmed that the electrodeposition mechanism of cobalt on ITO substrate follows the 3D nucleation instantaneous in nitrate solution and the 3D nucleation progressive in chloride solution. The Heerman-Tarallo model was used to analyze the evolution of kinetic parameters; it was found that the nucleation rate (*A*) and nuclei density (*N₀*) increase with the applied potential, and the diffusion coefficient can be considered independent of the potential. The cobalt electrodeposited from nitrate medium has cyan color and blue color using the chloride solution. The XRD characterization showed that the cobalt electrodeposited has a hexagonal structure whatever the electrolyte medium. However, the cobalt crystallites electrodeposited from the chloride solution have a larger size compared to that of the cobalt electrodeposited from the nitrate solution.

Acknowledgements This work is carried out at Bio-Geosciences and Materials Engineering laboratory at the ENS Casablanca, Morocco. The authors would like to thank all those who helped them to carry out the analysis at the XRD at the faculty of sciences Ain Chock, Casablanca.

References

- Lghazi Y, Moubah R, Bimaghra I, Hlil Ek, ElBahraoui T, Allegand S, Lasri H (2017) Investigation of structural and magnetic properties in electrodeposited Co/CoxZn1-x superlattices. *J Supercond Nov Magn* 30(9):2641–2645. <https://doi.org/10.1007/s10948-017-4075-8>
- Lee KK, Loh PY, Sow CH, Chin WS (2012) CoOOH nanosheets on cobalt substrate as a non-enzymatic glucose sensor. *Electrochem Commun* 20:128–132. <https://doi.org/10.1016/j.elecom.2012.04.012>

3. Chen M, Xia X, Zhang J, Qi M, Yin J, Chen Q (2016) Controllable synthesis of cobalt oxide nanoflakes on three-dimensional porous cobalt networks as high-performance cathode for alkaline hybrid batteries. *Mater Res Bull* 74:472–477. <https://doi.org/10.1016/j.materresbull.2015.11.025>
4. Yang Y, Fei H, Ruan G, Tour JM (2015) Porous cobalt-based thin film as a bifunctional catalyst for hydrogen generation and oxygen generation. *Adv Mater* 27(20):3175–3180. <https://doi.org/10.1002/adma.201500894>
5. Zhang L, Yang C, Zhao G, Mu J, Wang Y (2015) Self-supported porous CoOOH nanosheet arrays as a non-enzymatic glucose sensor with good reproducibility. *Sensors Actuators B Chem* 210:190–196. <https://doi.org/10.1016/j.snb.2014.12.113>
6. Wang X, Tian W, Zhai T, Zhi C, Bando Y, Golberg D (2012) Cobalt(II,III) oxide hollow structures: fabrication, properties and applications. *J Mater Chem* 22(44):23310–23326. <https://doi.org/10.1039/c2jm33940d>
7. Jiang J, Liu J, Ding R, Zhu J, Li Y, Hu A, Li X, Huang X (2011) Large-scale uniform α -Co(OH)₂ long nanowire arrays grown on graphite as pseudocapacitor electrodes. *ACS Appl Mater Interfaces* 3(1):99–103. <https://doi.org/10.1021/am1009887>
8. Hou Y, Kondoh H, Shimojo M, Kogure T, Ohta T (2005) High-yield preparation of uniform cobalt hydroxide and oxide nanoplatelets and their characterization. *J Phys Chem B* 109(41):19094–19098. <https://doi.org/10.1021/jp0521149>
9. Rios-Reyes CH, Mendoza-Huizar LH, Rivera M (2009) Electrochemical kinetic study about cobalt electrodeposition onto GCE and HOPG substrates from sulfate sodium solutions. *J Solid State Electrochem* 14(4):659–668. <https://doi.org/10.1007/s10008-009-0816-3>
10. Ait Himi M, El Ghachtouli S, Amarray A et al (2020) Removal of azo dye Calcon using polyaniline films electrodeposited on SnO₂ substrate. *Phys Chem Res* 8:111–124. <https://doi.org/10.22036/pcr.2019.203023.1680>
11. Miranda-Hernández M, Palomar-Pardavé M, Batina N, González I (1998) Identification of different silver nucleation processes on vitreous carbon surfaces from an ammonia electrolytic bath. *J Electroanal Chem* 443(1):81–93. [https://doi.org/10.1016/S0022-0728\(97\)00487-7](https://doi.org/10.1016/S0022-0728(97)00487-7)
12. Fletcher S, Halliday CS, Gates D, Westcott M, Lwln T, Nelson G (1983) The response of some nucleation/growth processes to triangular scans of potential. *J Electroanal Chem Interfacial Electrochem* 159(2):267–285. [https://doi.org/10.1016/S0022-0728\(83\)80627-5](https://doi.org/10.1016/S0022-0728(83)80627-5)
13. Mendoza-Huizar LH, Robles J, Palomar-Pardavé M (2003) Nucleation and growth of cobalt onto different substrates - Part II. The upd-opd transition onto a gold electrode. *J Electroanal Chem* 545:39–45. [https://doi.org/10.1016/S0022-0728\(03\)00087-1](https://doi.org/10.1016/S0022-0728(03)00087-1)
14. Bard AJ, Faulkner LR (1980) *Electrochemical method: fundamentals and applications*. Wiley, New York 91-92 and 500-511
15. Zhang C, Jiang L, Xu F, Duan N, Xin B, Han G, Zhang G, Wen Y (2018) New insight into cleaner control of heavy metal anode slime from aqueous sulfate electrolytes containing Mn (II): preliminary characterization and mechanism analysis. *J Clean Prod* 177:276–283. <https://doi.org/10.1016/j.jclepro.2017.12.252>
16. Mashreghi A, Zare H (2016) Investigation of nucleation and growth mechanism during electrochemical deposition of nickel on fluorine doped tin oxide substrate. *Curr Appl Phys* 16(5):599–604. <https://doi.org/10.1016/j.cap.2016.03.008>
17. Ait Himi M, El Ghachtouli S, Youbi B et al (2019) Nucleation and growth mechanism of manganese oxide electrodeposited on ITO substrate. *Mater Today Proc* 30:963–969. <https://doi.org/10.1016/j.matpr.2020.04.358>
18. Gupta A, Srivastava C (2020) Nucleation and growth mechanism of tin electrodeposition on graphene oxide: a kinetic, thermodynamic and microscopic study. *J Electroanal Chem* 861:113964. <https://doi.org/10.1016/j.jelechem.2020.113964>
19. Ait Ahmed N, Eyraud M, Hammache H, Vacandio F, Sam S, Gabouze N, Knauth P, Pelzer K, Djenizian T (2013) New insight into the mechanism of cathodic electrodeposition of zinc oxide thin films onto vitreous carbon. *Electrochim Acta* 94:238–244. <https://doi.org/10.1016/j.electacta.2013.01.103>
20. Youbi B, Lghazi Y, Ait Himi M et al (2020) Growth mechanism during the early stages of electrodeposition of bismuth telluride Bi₂Te₃ on ITO substrate. *Mater Today Proc* 30:842–848. <https://doi.org/10.1016/j.matpr.2020.04.338>
21. Lghazi Y, Bimaghra I, El Bachiri A, Elmerzouki K, Youbi B, Lasri H (2018) Investigation of the nucleation kinetics of Bi and Δ -Bi₂O₃ during electro-deposition on substrate ITO. *Int J Eng Technol* 7(4.32):21–24
22. Astley DJ, Harrison JA, Thirsk HR (1968) Electrocrystallization of mercury, silver and palladium. *Trans Faraday Soc* 64:192. <https://doi.org/10.1039/TF9686400192>
23. Gunawardena G, Hills G, Scharifker B (1981) Induction times for the formation of single mercury nuclei on a platinum microelectrode. *J Electroanal Chem* 130:99–112. [https://doi.org/10.1016/S0022-0728\(81\)80379-8](https://doi.org/10.1016/S0022-0728(81)80379-8)
24. Youbi B, Lghazi Y, El Bachiri A et al (2020) Investigation of nucleation and growth mechanism of bismuth electrodeposited on ITO substrate in nitric acid medium. *Mater Today Proc* 22:6–11. <https://doi.org/10.1016/j.matpr.2019.08.055>
25. Youbi B, Lghazi Y, Ait Himi M, Bimaghra I (2019) Nucleation and growth mechanism of tellurium electrodeposited on tin-doped indium oxide substrate. *J Appl Electrochem* 50(2):159–168. <https://doi.org/10.1007/s10800-019-01377-0>
26. Mezine Z, Kadri A, Hamadou L, Benbrahim N, Chaouchi A (2018) Electrodeposition of copper oxides (Cu_xO_y) from acetate bath. *J Electroanal Chem* 817:36–47. <https://doi.org/10.1016/j.jelechem.2018.03.055>
27. Scharifker B, Hills G (1983) Theoretical and experimental studies of multiple nucleation. *Electrochim Acta* 28(7):879–889. [https://doi.org/10.1016/0013-4686\(83\)85163-9](https://doi.org/10.1016/0013-4686(83)85163-9)
28. Heerman L, Tarallo A (1999) Theory of the chronoamperometric transient for electrochemical nucleation with diffusion-controlled growth. *J Electroanal Chem* 470(1):70–76. [https://doi.org/10.1016/S0022-0728\(99\)00221-1](https://doi.org/10.1016/S0022-0728(99)00221-1)
29. Alvarez AE, Salinas DR (2010) Formation of Cu/Pd bimetallic crystals by electrochemical deposition. *Electrochim Acta* 55(11):3714–3720. <https://doi.org/10.1016/j.electacta.2010.01.076>
30. Sluyters-Rehbach M, Wijenberg JHOJ, Bosco E, Sluyters JH (1987) The theory of chronoamperometry for the investigation of electrocrystallization. Mathematical description and analysis in the case of diffusion-controlled growth. *J Electroanal Chem* 236(1-2):1–20. [https://doi.org/10.1016/0022-0728\(87\)88014-2](https://doi.org/10.1016/0022-0728(87)88014-2)
31. Scharifker B, Mostany J (1984) Three-dimensional nucleation with diffusion controlled growth Part I. Number density of active sites and nucleation rates per site. *J Electroanal Chem* 177(1-2):13–23. [https://doi.org/10.1016/0022-0728\(84\)80207-7](https://doi.org/10.1016/0022-0728(84)80207-7)
32. Heerman L, Tarallo A (1998) Electrochemical nucleation on microelectrodes. Theory and experiment for diffusion-controlled growth. *J Electroanal Chem* 451(1-2):101–109. [https://doi.org/10.1016/S0022-0728\(98\)00101-6](https://doi.org/10.1016/S0022-0728(98)00101-6)
33. Palomar-Pardavé M, Scharifker BR, Arce EM, Romero-Romo M (2005) Nucleation and diffusion-controlled growth of electroactive centers: reduction of protons during cobalt electrodeposition. *Electrochim Acta* 50(24):4736–4745. <https://doi.org/10.1016/j.electacta.2005.03.004>
34. Deutscher RL, Fletcher S (1988) Nucleation on active sites. Part IV. Invention of an electronic method of counting the number of crystals as a function of time; and the discovery of nucleation rate dispersion. *J Electroanal Chem* 239(1-2):17–54. [https://doi.org/10.1016/0022-0728\(88\)80268-7](https://doi.org/10.1016/0022-0728(88)80268-7)

35. Yuan X, Hu XX, Ding XL, Kong HC, Sha HD, Lin H, Wen W, Shen G, Guo Z, Ma ZF, Yang Y (2013) Effects of cobalt precursor on pyrolyzed carbon-supported cobalt-polypyrrole as electrocatalyst toward oxygen reduction reaction. *Nanoscale Res Lett* 8(1):478. <https://doi.org/10.1186/1556-276X-8-478>
36. Premalatha S, Babu GNKR (2018) Direct current electrodeposition of Co-ITO nanoflakes modified steel electrode for highly selective non enzymatic detection of catechol. *J Alloys Compd* 767:622–631. <https://doi.org/10.1016/j.jallcom.2018.07.119>
37. Kidosaki T, Takase S, Shimizu Y (2012) Electrodeposited cobalt-iron alloy thin-film for potentiometric hydrogen phosphate-ion sensor. *J Sens Technol* 2(03):95–101. <https://doi.org/10.4236/jst.2012.23014>
38. Monshi A, Foroughi MR, Monshi MR (2012) Modified Scherrer equation to estimate more accurately nano-crystallite size using XRD. *World J Nano Sci Eng* 02(03):154–160. <https://doi.org/10.4236/wjnse.2012.23020>

Publisher's note Springer Nature remains neutral with regard to jurisdictional claims in published maps and institutional affiliations.